Available online at www.sciencedirect.com
SCIENCE DIRECT®
Quaternary International 154–155 (2006) 73–86

Late Quaternary landscape evolution in the Kunlun Mountains and Qaidam Basin, Northern Tibet: A framework for examining the links between glaciation, lake level changes and alluvial fan formation

Lewis A. Owen[a,*], Robert C. Finkel[b], Ma Haizhou[c], Patrick L. Barnard[d]

[a]Department of Geology, University of Cincinnati, Cincinnati, OH 45221-0013, USA
[b]Center for Accelerator Mass Spectrometry, Lawrence Livermore National Laboratory, Livermore, CA 94550, USA
[c]Institute of Saline Lakes, Chinese Academy of Sciences, Xining, Qinghai, P.R. China
[d]United States Geological Survey, Pacific Science Center, 400 Natural Bridges Drive, Santa Cruz, CA 95060, USA

Available online 13 March 2006

Abstract

The Qaidam Basin in Northern Tibet is one of the largest hyper-arid intermontane basins on Earth. Alluvial fans, pediment surfaces, shorelines and a thick succession of sediments within the basin, coupled with moraines and associated landforms in the adjacent high mountain catchments of the Kunlun Mountains, record a complex history of Late Quaternary paleoenvironmental change and landscape evolution. The region provides an ideal natural laboratory to examine the interaction between tectonics and climate within a continent–continent collision zone, and to quantify rates of landscape evolution as controlled by climate and the associated glacial and hydrological changes in hyper-arid and adjacent high-altitude environments. Geomorphic mapping, analysis of landforms and sediments, and terrestrial cosmogenic radionuclide surface exposure and optically stimulated luminescence dating serve to define the timing of formation of Late Quaternary landforms along the southern and northwestern margins of the Qaidam Basin, and in the Burhan Budai Shan of the Kunlun Mountains adjacent to the basin on the south. These dates provide a framework that suggests links between climatic amelioration, deglaciation, lake desiccation and alluvial fan evolution. At least three glacial advances are defined in the Burham Budai Shan of the Kunlun Mountains. On the northern side of this range these occurred in the penultimate glacial cycle or early in the last glacial cycle, during the Last Glacial Maximum (LGM)/Lateglacial and during the Holocene. On the south side of the range, advances occurred during the penultimate glacial cycle, MIS-3, and possibly the LGM, Lateglacial or Holocene. Several distinct phases of alluvial fan sedimentation are likewise defined. Alluvial fans formed on the southern side of the Kunlun Mountains prior to 200 ka. Ice-contact alluvial fans formed during the penultimate glacial and during MIS-3. Extensive incised alluvial fans that form the main valley fills north of the Burham Budai and extend into the Qaidam Basin are dated to ~30 ka. These ages suggest that there was a period of alluvial fan aggradation and valley filling that persisted until desiccation of the large lakes in the Qaidam Basin post ~30 ka led to base level lowering and active incision of streams into the valley fills. The continued Lateglacial and Holocene desiccation likely led to further degradation of the valley fills. Ice wedge casts in the Qaidam Basin date to ~15 ka, indicating significant Lateglacial climatic amelioration, while Holocene loess deposits north of the Burham Bdudai suggest that aridity has increased in the region since the early Holocene. From these observations, we infer that the major landscape changes within high glaciated mountains and their adjacent hyper-arid intermontane basins, such as the Kunlun Mountains and Qaidam Basin, occur rapidly over millennial timescales during periods of climatic instability.

1. Introduction

The Qaidam Basin is a tectonically controlled depression on the northern margin of the Tibetan Plateau (Fig. 1). The hyper-arid basin floor has an average altitude of ~2700 m asl and while the bordering mountains of the Kunlun, Aljun and Qilian Shan rise to over 5000 m asl and are extensively glaciated (Chen and Bowler, 1986; Wang et al., 1986; Brantingham et al., 2001, 2003; Fig. 2). Abundant salt deposits are present within the basin, and together with other intermontane basin sediments and landforms these

*Corresponding author. Tel.: +1 513 556 4203; fax: +1 513 556 6931.
E-mail address: lewis.owen@uc.edu (L.A. Owen).

1040-6182/$ - see front matter
doi:10.1016/j.quaint.2006.02.008

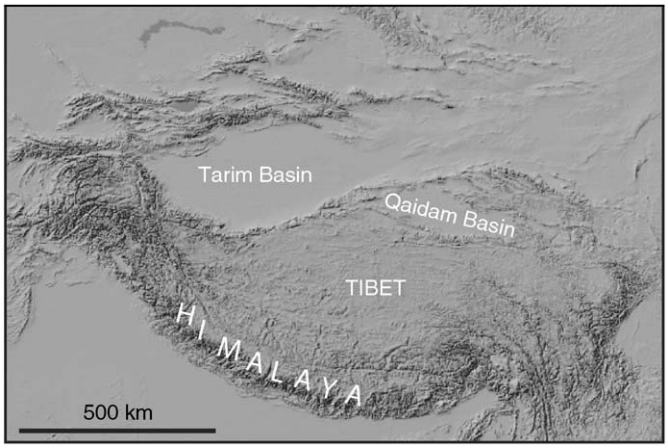

Fig. 1. Digital elevation model showing the location of the Qaidam Basin in Tibet. The main study area is highlighted by the box.

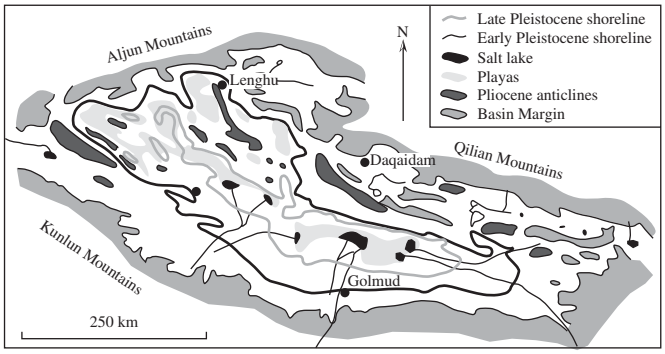

Fig. 2. Outline of the Qaidam Basin showing the extent of early and late Pleistocene mega-lakes as proposed by Chen and Bowler (1986). The main detailed study areas within the Qaidam Basin are highlighted by the black boxes.

record a history of environmental change and fluctuating lake levels throughout the Quaternary (Figs 2 and 3). The Qaidam Basin, therefore, provides a natural laboratory for examining the nature of intermontane basin evolution within a continent–continent collision zone, and for quantifying rates of landscape evolution and paleoenvironmental change in a hyper-arid environment. Landforms within the adjacent high mountains allow former glaciations to be reconstructed, and suggest linkages between glaciations and the formation of landforms such as alluvial fans and terraces.

Along the margins of the basin, pediments and impressive deeply incised alluvial fans radiate from the mountains grading towards ancient lake shorelines (Fig. 3). Chen and Bowler (1986) suggested that these shorelines represent mega-lakes that filled the Qaidam Basin during the early and late Pleistocene (Figs 2, 3 and 4). Unfortunately, Chen and Bowler (1986) were unable to adequately define the timing of the formation of the lake because of the general absence of organic material for radiocarbon dating, essentially the only technique available

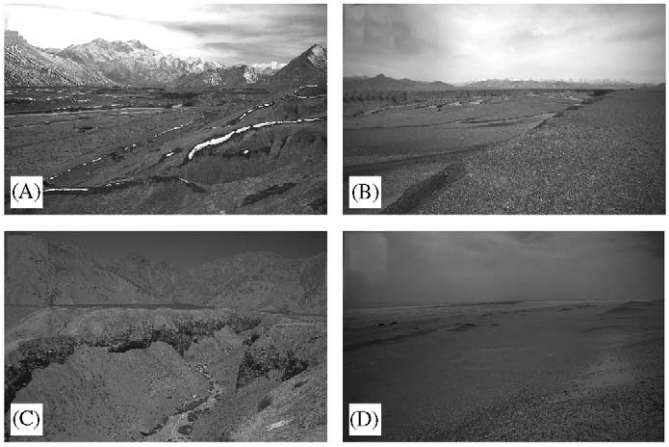

Fig. 3. Views of the dominant landforms within the study area. (A) Incised alluvial fans radiating from the glaciated mountains of the Kunlun. (B) Alluvial fans and active channels near Golmud. These were probably incised due to base-level lowering as lake level dropped at the end of MIS-3. (C) Typical sections within alluvial fans near Golmud. These exposures allow easy access to examine the fan sedimentology. Typical graphic sedimentary logs within such a fan succession is shown in Fig. 7. (D) Late Pleistocene shorelines near Lenghu. A typical section within such a shoreline is shown in Fig. 9.

Fig. 4. Location of study sites in the Kunlun Mountains and adjacent Qaidam Basin.

at that time, and the limited time range (~30–40 ka) of the radiocarbon technique. As a result, they could only speculate on the age of the earliest mega-lake. However, on the basis of limited radiocarbon dating, they suggested that the late Pleistocene mega-lake formed during humid conditions that persisted until after 30–40 ka (latter half of marine isotope stage 3 [MIS-3]), with the lake desiccating

from about 25–9 ka. Expanded lake level during MIS-3 is supported by the coring of Wang et al. (1986) in the Dabusan Lake in the central Qaidam Basin. Furthermore, reconstruction from lake levels and other geologic proxy throughout other regions of Tibet suggest that the Indian monsoon was enhanced between 30 and 40 ka (Shi et al., 2001). Recent work on the glacial history of Tibet and the bordering mountains supports this view with glaciers advancing to their maximum extent during MIS-3 and with reduced glaciation during the latter part of the last glacial cycle when moisture supply was more restricted (Richards et al., 2000a, b; Owen et al., 2001, 2002a, b, c, 2003a, b, c; Finkel et al., 2003). This suggests that there is a strong link between times of climatic amelioration, deglaciation, lake desiccation and alluvial fan sedimentation, and that major landscape changes take place very rapidly over short intervals of time during periods of climatic instability. Similar patterns of landscape evolution are evident in the monsoon-influenced mountains of the Himalaya (Barnard et al., 2004a, b).

To test this relationship in a hyper-arid setting, we studied the Qaidam Basin, and the adjacent Burhan Budai Shan in the Kunlun Mountains by undertaking remote sensing, field mapping, geomorphological and sedimentological analysis, and numerical dating of Late Quaternary landforms and sediment. In particular, we undertook a program of optically stimulated luminescence (OSL) and terrestrial cosmogenic radionuclide surface exposure dating (SED) to define the timing of formation of Late Quaternary landforms. This allows us to test our hypothesis that the formation of landforms is synchronous with times of climatic instability and that landforms develop rapidly over relatively short periods of time and examine the spatial context of landforms within these settings.

2. Methods

2.1. Fieldwork

Field work was undertaken in the Burhan Budai Shan of the Kunlun Mountains and in the Qaidam Basin. Detailed studies were carried out at locations on the southern and northern sides of the Burhan Budai Shan, the main drainage of the Burhan Budai that flows northern to Golmud, Xiao Qaidam, and Lenghu (Fig. 4). This allowed us to examine the relationship between the glacial records in the Kunlun and to follow the alluvial fan successions into the basin to the shorelines. The moraines, alluvial fans, pediments and terraces were examined and correlated morphostratigraphically, and mapped using the standard techniques of Derbyshire and Owen (1990) and aided by remote sensing. The geomorphology and sedimentology of the alluvial fans, terraces and pediments were examined by constructing lateral and vertical graphic sedimentary logs using methods similar to those described in Benn and Owen (2002).

Sediment samples for OSL dating were collected by hammering light tight tubes into freshly exposed sediments. The tubes remained sealed until processed in the safe light conditions at the Luminescence Dating Laboratory at University of California, Riverside. Samples for SED dating were collected by chiseling off ~500 g of rock from the upper surfaces of quartz-rich boulders along moraine crests on alluvial fans. Locations were chosen where there was no apparent evidence of exhumation or slope instability. The largest boulders were chosen to help reduce the possibility that boulders may have been covered with snow for significant periods (several months) of the year. To provide a check on the reproducibility of the dating and to check for the possibility of inheritance of terrestrial cosmogenic radionuclides (TCNs), where possible, several boulders were sampled from each moraine ridge and alluvial fan. The degree of weathering and the site conditions for each boulder were recorded. Topographic shielding was determined by measuring the inclination from the boulder site to the top of the surrounding mountain ridges and peaks.

2.2. Optically stimulated luminescence dating

OSL measurements were undertaken at the Luminescence Dating Laboratory at the University of California, Riverside. The in situ water content (mass of moisture/dry mass; Aitken, 1998) was determined by drying sub-samples in an oven at 50 °C. The sample for dating was dry-sieved to obtain a 90–125 μm particle size fraction. The carbonates and organic matter were removed from the 90–125 μm fraction using 10% HCl and 30% H_2O_2, respectively. Sodium polytungstate solutions of different densities and a centrifuge were used to separate the quartz and feldspar-rich fractions from the heavy minerals. The separated quartz-rich fraction was treated with 49% HF for 80 min to dissolve any plagioclase feldspars and remove the alpha-irradiated surface of the quartz grains. Dried quartz grains were mounted on stainless steel discs with silicon spray. All the preparation techniques were carried out under laboratory safelights to avoid sample bleaching.

Approximately 20 g of the dried sub-sample from the sediment sample was ground to a fine powder and sent to the Becquerel Laboratories at Lucas Heights in Australia for INAA. Using dose-rate conversion factors of Adamiec and Aitken (1998) and beta attenuation factors of Mejdahl (1979) and Adamiec and Aitken (1998), the elemental concentrations were converted into external beta and gamma components, which were in turn attenuated for moisture content. These were summed together with a cosmic ray component using the methods of Prescott and Hutton (1994) to give estimates of the total dose-rate for each sample (Table 1). The water content throughout the section may have occurred throughout the history of the section, varied, but it is difficult to determine the degree of such changes; we have assumed a constant dose-rate, but

Table 1
Instrumental neutron activation analysis, cosmic dose rates, total doses and ages

Sample #/Lab ID	Sediment type[a]	K (%)[b]	Rb (ppm)[b]	Th (ppm)[b]	U (ppm)[b]	Water content (%)[c]	Cosmic dose rate (Gy/ka)[d]	Total dose rate (Gy/ka)[e]	Number of aliquots	D_E (Gy)[f]	Age (ka)
QD8 (257)	CGQ-A	2.06	89.5	8.28	1.93	5	0.37±0.04	3.24±0.20	32	85.56±19.97	26.3±2.4
QD4A (258)	CGQ-B	1.65	90.0	12.10	2.46	5	0.31±0.03	3.20±0.18	16	27.40±4.15	8.6±0.7
QD2 (259)	CGQ-B	1.78	75.6	9.52	2.16	5	0.31±0.03	3.07±0.18	16	86.19±15.91	28.3±2.8
QD7A (260)	CGQ-B	1.85	81.1	11.20	1.56	5	0.32±0.03	3.12±0.19	16	27.32±6.32	8.8±0.8
QBOSL6A (262)	CGQ-A	1.05	65.1	5.28	1.14	5	0.32±0.03	1.99±0.12	12	29.70±6.43	14.9±1.5

[a]Analysis for coarse-grained (90–125 μm) quartz fraction (CGQ) on (A) poorly sorted sand and (B) pebbly sand.
[b]Uncertainties on analyses of U, Th, Rb and K are taken to be ±10%.
[c]Uncertainty taken as ±5%.
[d]Cosmic doses and attenuation with depth were calculated using the methods of Prescott and Stephans (1982) and Prescott and Hutton (1994).
[e]Total doses combine the cosmic dose rate and the beta and gamma doses calculated from the K, Rb, Th and U concentrations in the sediment using the methods of Adamiec and Aitken (1998) and Mejdahl (1979) with corrections for moisture content after Zimmerman (1971).
[f]Average equivalent dose (D_E) and error ($1\sigma_{n-1}$ of the D_E), incorporating the error from beta source estimated at about ±5%.

have used 10±5% water content to help compensate for possible changes in water content.

Luminescence measurements were undertaken using a Daybreak 1100 automated system with an 1100FO/L combined fiber-optic/IRLED illuminator for optical stimulation (Bortolot, 1997). Luminescence from the quartz grains was stimulated using a 150 W halogen lamp producing green light (514±34 nm; ~20 mW cm^{-2}) defined by an additional narrow band interference filter. All quartz samples were screened for feldspar contamination using infrared stimulation from T-1 GaAlAs diodes (880±80 nm; diode current, 20 mA). All OSL signals were detected with a photomultiplier tube characterized by 9 mm Schott UG11 ultraviolet detection filters. Daybreak TLApplic 4.30 software was used for hardware control and equivalent dose (D_E) analysis.

D_E measurements were determined on multiple aliquots for each sample using the single aliquot regenerative (SAR) protocol developed by Murray and Wintle (2000). In the SAR method, each natural or regenerated OSL signal is corrected for changes in sensitivity using the OSL response to a subsequent test dose. The natural dose (N) was measured in the first cycle, and thereafter five regeneration doses (R_1 to R_5) were administered. The first three were used to bracket the natural luminescence level ($R_1 < N \sim R_2 < R_3$), the fourth (R_4) was set at zero to monitor recuperation (i.e. R_4/N) and to monitor the reproducibility of sensitivity corrections and the fifth dose was equal to the first dose (i.e. R_5/R_1). Each measurement cycle comprised a regeneration dose (zero for natural), preheating of 220 °C for 10 s, optical stimulation for 100 s (sample temperature of 125 °C), a constant test-dose, a test-preheat of 160 °C for 0 s and a final optical stimulation for 100 s (at 125 °C). The net-natural and net-regenerated OSL were derived by taking the initial OSL signal (0–1 s) and subtracting a background from the last part of the stimulation curve (90–100 s); subtracting the background from the preceding natural and regenerative OSL signals derived the net test-dose response. Growth curves were plotted using the net natural and regenerated data divided by the subsequent response to the net test-dose. The growth curve data was fitted with either a single saturating exponential. The D_E for each sample was calculated using the mean values and standard error of all the aliquots for each sample (Table 1). Probability plots were constructed to illustrate the spread of D_E values for each sample and support the use of a mean and standard error to calculate the OSL age for each sample. The INAA, cosmic dose rates, total doses, mean D_E and OSL ages are shown in Table 1.

2.3. Laboratory methods for SED dating

First, the samples were crushed and sieved. Quartz was then separated from the 250–500 μm size fraction using the method of Kohl and Nishiizumi (1992). After addition of Be carrier, Be was separated and purified by ion exchange chromatography and precipitation at pH > 7.

The hydroxides were oxidized by ignition in quartz crucibles. BeO was then mixed with Nb metal prior to determination of the $^{10}Be/^{9}Be$ ratios by accelerator mass spectrometry at the Center for Accelerator Mass Spectrometry in the Lawrence Livermore National Laboratory. Isotope ratios were compared to ICN ^{10}Be standards prepared by K. Nishiizumi (pers. comm. 1995) using a half life of 1.5×10^6 yr.

The measured isotope ratios were converted to TCN concentrations in quartz using the total Be in the samples and the sample weights. Radionuclide concentrations were then converted to zero-erosion exposure ages using sea level high latitude (SLHL) ^{10}Be production rate of 5.16 at g^{-1} quartz^{-1} yr (Stone, 2000). The Be production rate used is based on a number of independent measurements as discussed by Owen et al. (2001, 2002a). Production rates were scaled to the latitude and elevation of the sampling sites using the star scaling factors of Lal and Peters (1967), Lal (1991) and Stone (2000) and an assumed 3% SLHL muon contribution. Incorporating changes in the paleomagnetic field would change the apparent exposure age by up to 10% for ages <100 ka. However, there is considerable debate regarding the technique and magnitude of this correction (Nishiizumi et al., 1996; Masarik and Wieler, 2003; Pigati and Lipton, 2004). We, therefore, present geomagnetically corrected ages in Table 1, but in the discussion that follows we use the ages that are not corrected for fluctuations in the paleomagnetic field. Details of the calculation are given in Farber et al. (2005).

3. Study areas

3.1. Burhan Budai Shan, Kunlun Mountains

Lui et al. (2006) describes the glacial geology of the Kunlun Pass area in the central Burhan Budai Shan and summarizes the work undertaken by Chinese scientists, who recognize evidence for three major glaciations: the Wangkun, Yakou and Yuzhufeng Glaciations, which are TL and ESR dated to 600–700, ~260 and 61–13 ka, respectively. We examined the glacial successions were examined in two valleys; one on the southern side of the Burhan Budai Shan approximately 10 km east of the Golmud-Lhasa highway; the other on the northern side of the Burhan Budai Shan south of the town of Xidatan (Fig. 4). The locations of the moraines and sampling sites for each of the study areas are shown in Figs. 5 and 6.

3.1.1. South side of the Burhan Budai Shan

Extensive glacial outwash alluvial fans form a bajada along the southern side of the Burhan Budai Shan. At least three distinct sets of alluvial fans are present (Fig. 5). The oldest comprises dissected alluvial fan remnants that rise 5–10 m above the younger onlapping alluvial fans. These fans are collectively referred to as F1. The surfaces of these alluvial fans are relatively smooth and have scattered boulders up to 2 m in diameter. The surface boulders are generally weathered with pits up to several tens of centimeters in diameter and several centimeters deep. Boulders that appeared to be least weathered (e.g. few pits) were sampled for SED (PR110–PR113). The next set of alluvial fans is very extensive, radiating from the tributary glaciated valleys of the Burhan Budai Shan. The heads of these alluvial fans terminate in steep proximal faces that slope up valley and trace out broad arcs, which radiate from the tributary valleys. In our study valley, the proximal slopes be can be traced to a high lateral moraine (M1) that rises several tens of meters above the western side of the contemporary drainage, well beyond the main mountain front. This relationship suggests that these landforms may have been ice-contact outwash fans. The surfaces of these fans are also relatively smooth and have

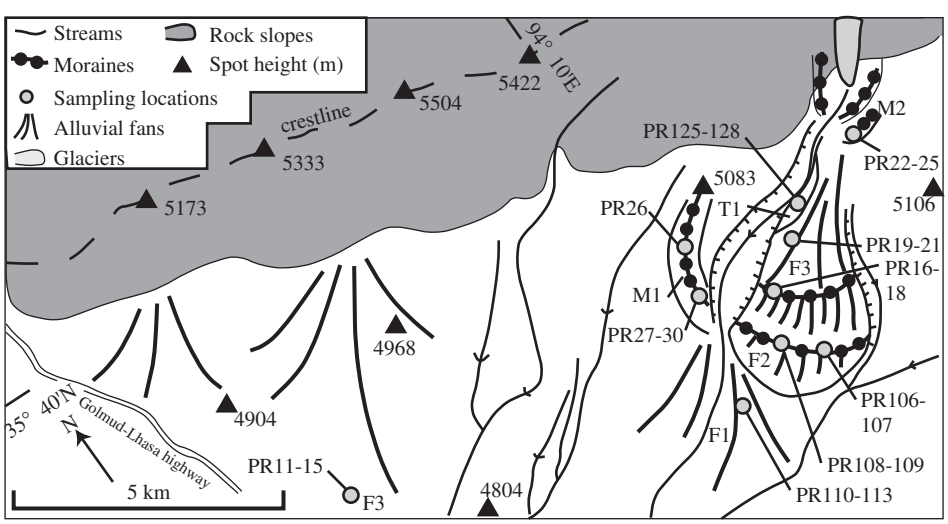

Fig. 5. Moraines along the southern side of the Burhan Budai Shan. The fan surfaces are labeled F1–F3, the moraines are M1 and M2, and the dated river terrace is T1.

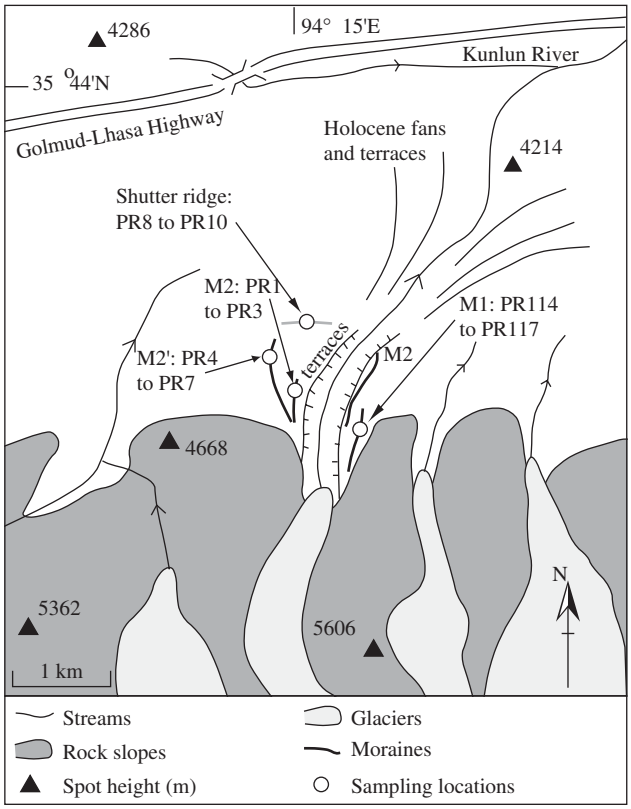

Fig. 6. Moraines and fans along the northern side of Burhan Budai Shan near Xidatan.

scattered boulders, which exhibit similar degrees of weathering as the higher dissected fan remnants; these are referred to as the F2 ice-contact outwash fans. Samples for SED were collected from both the moraine and the outwash fan (PR16–PR18, PR106 and PR109; PR26–PR30).

The next set of alluvial fans, referred to as the F3 fans, has an undulating surface of subdued channels and levees and has a higher frequency of surface boulders than F1 and F2. Samples for SED were collected from boulders within the study valley (PR19–PR21) and from a surface ~10 km to the west of the main study valley (PR11–PR15). In our study valley F3 originated at a latero-frontal moraine, which rises several tens of meters above the contemporary drainage within the tributary valley. A set of samples for SED were collected from this moraine (M2; PR22–PR25).

Near the contemporary stream, an F3 alluvial fan overlies a river terrace. This terrace rises several meters above the contemporary stream. In contrast to the outwash and ice-contact fans, it contains no surface boulders; however, well-rounded cobbles are abundant. We collected cobble samples (PR125–PR128) for SED from this terrace and refer to it as T1. Morphostratigraphically, this should be the youngest landform we attempted to date in this study area.

A younger moraine is present up valley of this moraine and encloses the contemporary glacier. This moraine was not dated.

3.1.2. North side of the Burhan Budai Shan

Several sets of alluvial fans are present along the northern side of the Burhan Budai Shan forming a bajada. These were mapped by Van der Woerd et al. (2002) and dated using SED methods. They showed that these formed during the Holocene and recognized five terraces at 8–9, 5–6, ~3, ~2 and < 1.5 ka. Two sets of moraines are evident near the exit of the tributary valleys. The older higher moraine we call M1 while the younger moraines are M2. The contemporary glaciers are only several kilometers from both these sets of moraines. In our study valley, the M1 moraine set is represented by subdued ridges near the exit of the tributary valley from the Burhan Budai Shan (Fig. 6). These rise more than 50 m above the contemporary drainages. The younger set of moraines (M2) is represented by several subdued ridges that rise several tens of meters above the contemporary drainage. The outermost one (M2′) can be traced to a shutter ridge that has been displaced by the Kunlun Fault. Surface boulders are not abundant on these surfaces and many may have been covered with a decimeter-thick layer of loess. We only sampled surface boulders that we believed are large enough and are located in positions where a simple unshielded exposure was most likely. Samples for SED (PR1–PR10 and PR114–PR117) were collected from each of the moraines and the shutter ridge. Small sharp crested lateral moraines are present near the contemporary glaciers at some locations within the valley.

3.2. Burhan Budai-Golmud drainage

The Lhasa-Golmud highway follows the main drainage (Kunlun River) of the Burhan Budai Shan from Xidatan to Golmud. Impressive alluvial fans are present along this drainage. These are incised at their toes and to their heads, rising many tens of meters above the contemporary drainage to form a notable valley fill and terrace-like landforms (Fig. 3). The alluvial fan surfaces coalesce and are almost continuous from Xidatan to Golmud eventually joining with the main bajada that stretches along the southern margin of the Qaidam basin. The alluvial fans comprise of crudely stratified meter and decimeter beds of fanglomerates and debris flows, and in places stratified sands and silts are present representing shallow ponds/swamps (Fig. 7). Older highly dissected alluvial fans are present along several stretches of the valley, but these are many tens of meters above the dominant alluvial fans that form the main valley fill (e.g. 35°55′N/094°40′E).

The deep fan incision has extended into the bedrock at some locations. At 35°53′N/094°45′E, for example, 3–4 m-thick the alluvial fans cap bedrock that has been incised by more than 25 m to form impressive strath terraces (Fig. 4). Samples for SED (PR100, PR101 and PR102) were collected from boulders on the alluvial fan surface. Other SED samples were collected from alluvial fan surfaces north of this location at 36°05′N/094°49′E (PR103) where an impressive alluvial fan radiating form a tributary valley

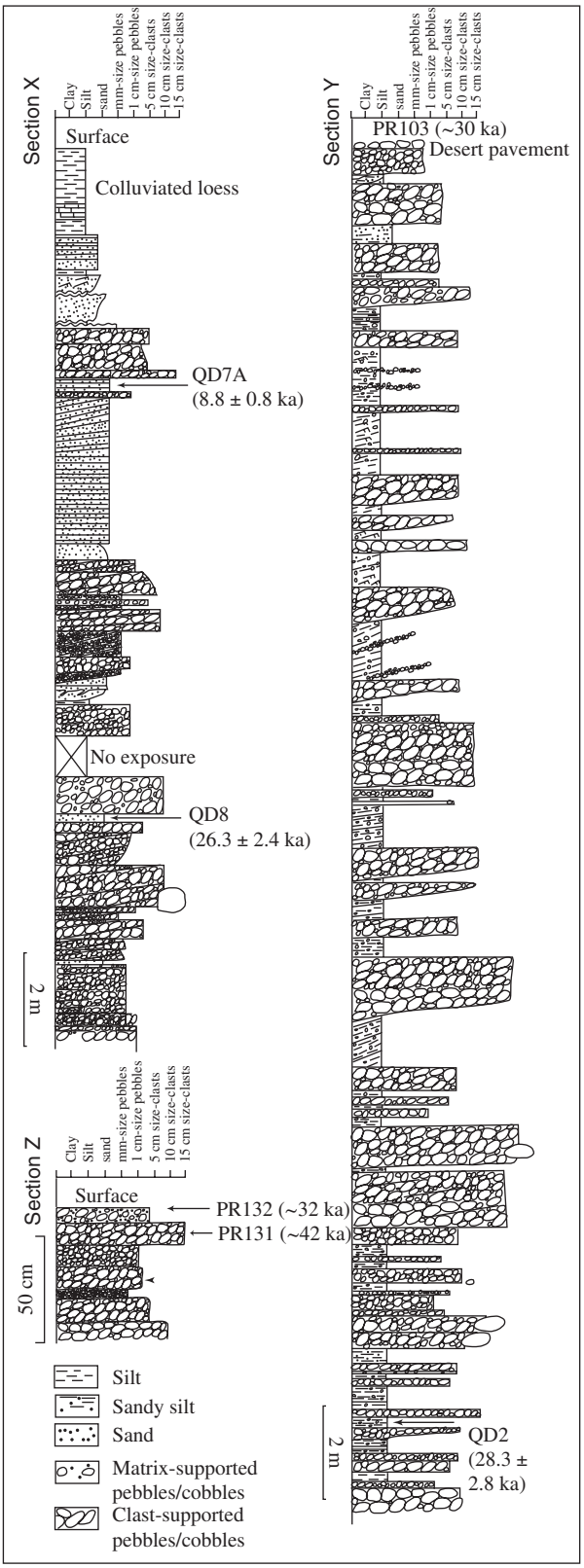

Fig. 7. Graphic sedimentary logs through a discontinuous valley fill/fan deposit ~50 km south of Golmud (36°04.749′N/094°48.325′E, 3245 m asl). Fig. 4 shows the locations of the sedimentary sections.

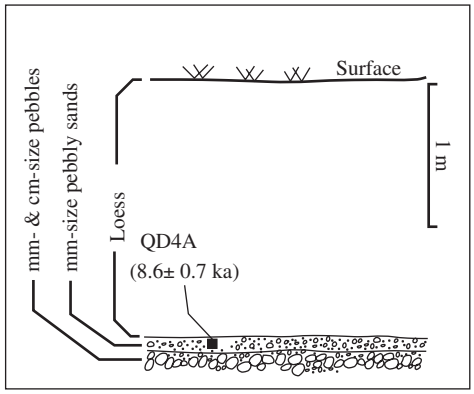

Fig. 8. Loess section covering an alluvial fan in the Golmud valley (35°55.480′N/094°40.080′E, 3631 m asl).

coalesces with the alluvial fans of the main drainage, and at 36°18′N/094°48′E near Golmud (Fig. 4).

A discontinuous deposit of loess, decimeters- to meters-thick, cap these alluvial fans and rock slopes throughout the valley. The thickest loess deposit we could observe is shown in Fig. 8. To date the age of the alluvial fans and to define the timing of fan incision, samples for OSL and CRN dating were collected from several locations which are shown in Fig. 7.

3.3. Xiao Qaidam

Xiao Qaidam is a small saline lake located ~50 km north of Golmud. Ancient shorelines are present along its southern margin representing former high stands. Fig. 9 shows a typical section through part of these shorelines. Paleolithic artifacts are present on the shorelines, mainly cores and flakes, which are believed to date to high lake level stands at ~30 ka. (Brantingham et al., 2003). The shorelines are incised by ~3 m deep ephemeral channels that grade to the present lake level.

3.4. Lenghu

A series of impressive shorelines are present near Lenghu (Fig. 3). The highest shoreline can be traced for at least a kilometer between two buttes at an altitude of ~2820 m asl at 38°51.3′N/093°26.3′E. This shoreline is constructed of clast-supported large discoidal pebbles and cobbles in a sandy matrix. A section through a shoreline ~5 m below the highest shoreline is shown in Fig. 10. The shorelines are discontinuous throughout the region because they are either eroded by ephemeral channels or buried by alluvial fans deposits. The alluvial fans above the highest shorelines near Lenghu have well-developed desert pavements with abundant ventifacts. Ice wedge casts are present in some of these shorelines filled with aeolian sands (Fig. 11). Cryoturbation structures are also present within the shoreline deposits (e.g., at 38°50.519′N/093°24.811′E 2785 m asl). These comprise involutions that have

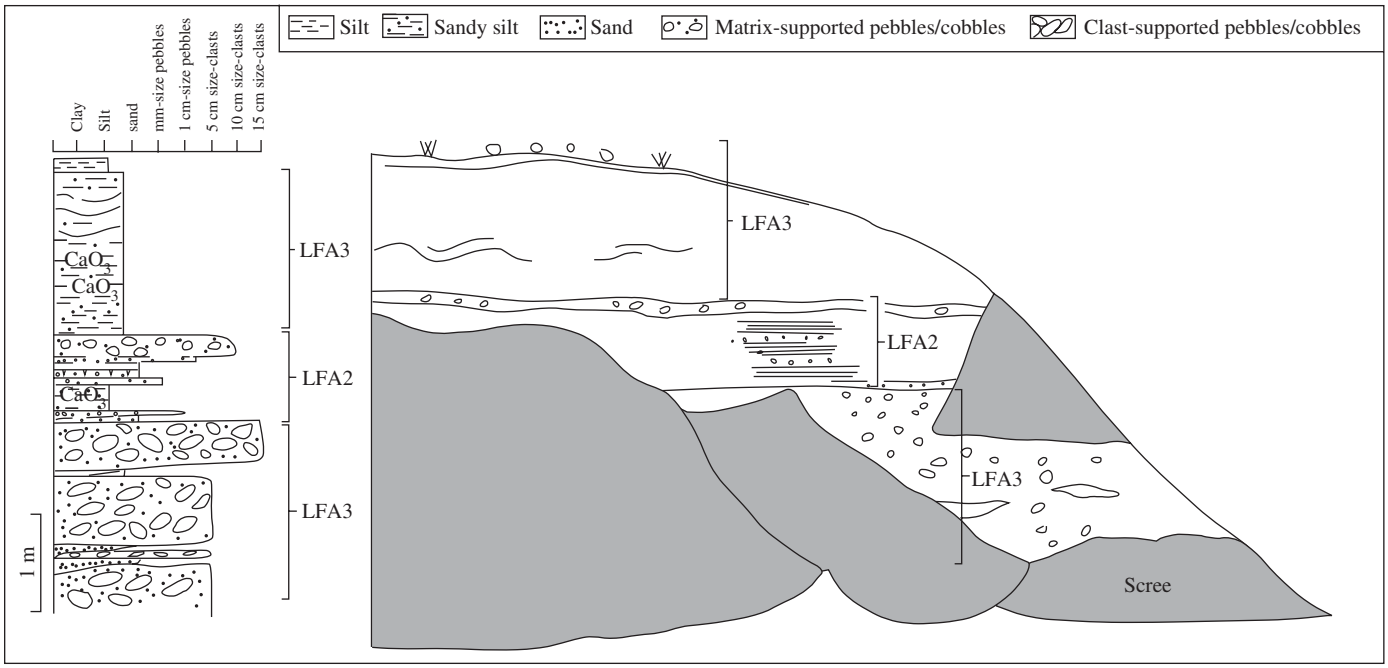

Fig. 9. Section within Late Quaternary beach complex at Daqaidam. The samples we have collected here will be dated using OSL and CRN methods and will help provide both a paleoenvieonmental and archaeological framework for the region. LFA—lithofacies associations. LFA1—storm beach pebbles and cobbles; LFA2—beach face pebbles, sands and silts; LFA3—shallow lake silty sands.

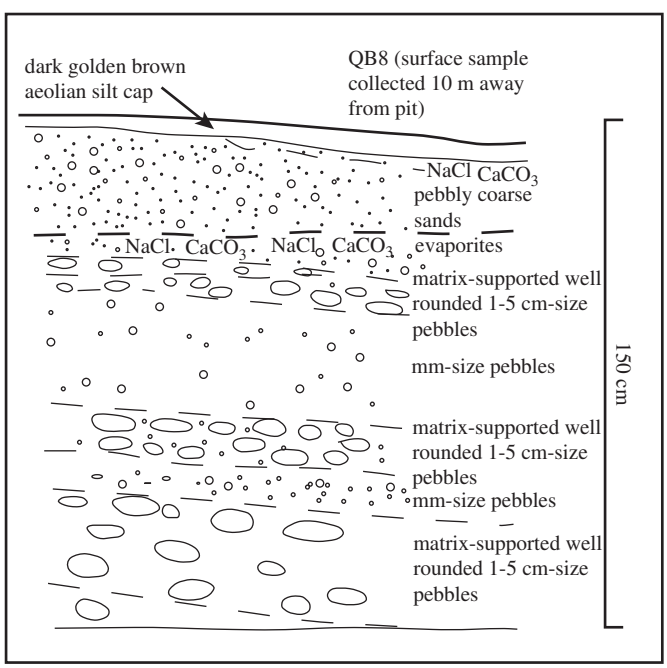

Fig. 10. Typical section showing the sedimentology of a beach ridge at Lenghu.

wavelengths and amplitudes that range from several cm to many decimeters.

4. Dating results

The dating results are shown in Tables 1 and 2, and on Figs. 7, 8, 11 and 12. All the samples that were dated using OSL methods were well-behaved, having bright luminescence signals (>10 times background levels) and most aliquots had a small recuperation (< 5%). With the exception of sample QBOSL6A, all the samples had dose rates of $\sim 3\,\mathrm{Gy\,ka^{-1}}$, a typical dose rate for desert environments (Table 1). The lower dose rate for sample QBOSL6A, may be due to a higher concentration of quartz within the sediment than for the other samples, which essentially dilutes the concentration of radioisotopes in the surrounding sediment.

The spread of SEDs for each surface is relatively large and is probably a consequence of: (1) inheritance of TCN in previously exposed surfaces; (2) weathering of surfaces; (3) shielding due to burial by sediment and/or snow and (4) when dating boulders, toppling of unstable boulders. Plotting the SEDs by relative ages of each surface as shown in Fig. 12 allow a qualitative assessment of the potential likelihood of spurious ages due to weathering, exhumation and/or toppling of boulders, and/or derivation of TCN from derived boulders. No correction has been applied for the uncertainty in the production rates of TCN, which may be in the order of ~5%. Furthermore, no correction is made for weathering of surfaces. However, for weathering rates of $1–5\,\mathrm{m\,Ma^{-1}}$, an exposure age of 10 ka, would underestimate the true age by 1–4%; an age of 20 ka, by 2–9%; an age of 50 ka, by 4–20%; an age of 100 ka, by 10–36%; an age of 200 ka, by 15–54%; and an age of 300 ka, by 23–56%. Weathering rates may vary considerably across the study areas, from possibly $<1\,\mathrm{m\,Ma^{-1}}$ in the arid regions of the Qaidam Basin to several $\mathrm{m\,Ma^{-1}}$ in the glaciated regions. Inheritance of TCN in boulders in

Table 2
Cosmogenic radionuclide data

Sample name	Latitude/longitude		Altitude (m)	Scaling factor correction	Depth/ topography correction	^{10}Be (10^6 atoms/ g^{-1})[a]	Be^{10} age (yr)	Be^{10} age with geomagnetic correction (yr)
PR1	35°42.3′	94°15.0′	4546	17.7	0.97	0.531±0.056	6028±637	6311±667
PR2	35°42.3′	94°15.0′	4548	17.71	0.97	1.297±0.058	14748±656	14852±661
PR3	35°42.2′	94°15.0′	4588	18.06	0.97	0.619±0.037	6893±411	7083±422
PR4	35°42.2′	94°14.9′	4610	18.25	0.97	1.149±0.048	12671±527	12818±533
PR5	35°42.2′	94°14.9′	4618	18.32	0.97	2.004±0.094	22072±1031	21738±1015
PR6	35°42.2′	94°14.9′	4620	18.33	0.97	1.116±0.050	12258±551	12397±557
PR7	35°42.2′	94°14.9′	4618	18.32	0.97	0.723±0.042	7933±457	8018±462
PR8	35°42.6′	94°14.7′	4475	17.1	0.97	7.637±0.173	91548±2078	83965±1906
PR9	35°42.9′	94°14.8′	4420	16.65	0.97	3.425±0.089	41688±1082	38353±996
PR10	35°42.9′	94°15.1′	4418	16.64	0.97	1.609±0.048	19497±581	19340±576
PR11	35°37.0′	94°5.1′	4793	19.85	0.97	3.116±0.076	31747±772	30299±736
PR12	35°37.1′	94°5.1′	4799	19.9	0.97	7.845±0.181	80589±1863	73787±1705
PR13	35°37.1′	94°5.1′	4807	19.98	0.97	4.100±0.095	41588±959	38268±882
PR14	35°37.2′	94°5.2′	4803	19.94	0.97	3.830±0.122	38894±1242	36259±1158
PR15	35°37.3′	94°5.2′	4812	20.03	0.97	3.652±0.086	36918±872	34716±820
PR16	35°36.5′	94°11.3′	4945	21.28	0.97	12.784±0.177	124050±1718	111018±1537
PR17	35°36.5′	94°11.3′	4945	21.28	0.97	2.588±0.081	24548±764	23964±746
PR18	35°36.5′	94°11.6′	4958	21.41	0.97	23.438±0.359	231700±3552	204433±3134
PR19	35°37.1′	94°11.8′	5027	22.1	0.97	4.225±0.059	38727±541	36137±504
PR20	35°37.1′	94°11.8′	5027	22.1	0.97	2.865±0.093	26179±846	25458±823
PR21	35°37.1′	94°11.8′	5023	22.06	0.97	3.338±0.072	30591±656	29292±628
PR22	35°37.8′	94°12.7′	5098	22.82	0.97	4.643±0.088	41228±785	37993±723
PR23	35°37.8′	94°12.7′	5104	22.88	0.97	2.941±0.054	25955±474	25258±461
PR24	35°37.8′	94°12.8′	5113	22.98	0.97	1.875±0.039	16440±345	16466±345
PR25	35°37.8′	94°12.8′	5113	22.98	0.97	1.293±0.028	11322±249	11449±252
PR26	35°37.6′	94°10.3′	5036	22.19	0.97	4.298±0.078	39225±713	36510±664
PR27	35°37.2′	94°10.0′	5020	22.03	0.97	16.143±0.303	152335±2860	134602±2527
PR28	35°37.1′	94°10.1′	5008	21.91	0.97	1.672±0.035	15377±326	15461±328
PR29	35°37.1′	94°10.0′	5016	21.99	0.97	5.395±0.107	49816±989	44767±889
PR30	35°37.0′	94°10.0′	4995	21.78	0.97	10.128±0.202	95417±1903	87572±1747
PR100	35°53′	94°44.8′	3471	10.19	0.97	1.249±0.040	24740±785	24098±765
PR101	35°53′	94°44.8′	3457	10.11	0.97	0.598±0.085	11896±1702	11991±1715
PR102	35°54′	94°44.9′	3495	10.33	0.97	0.511±0.043	9957±838	9972±839
PR103	35°4.5′	94°48.7′	3270	9.14	0.97	1.401±0.078	30989±1726	29612±1649
PR106	35°36′	94°10.8′	4924	21.08	0.97	21.153±0.482	211427±4820	188000±4286
PR107	35°36′	94°10.7′	4932	21.16	0.97	21.906±0.546	218509±5445	193122±4813
PR108	35°37′	94°11.6′	4967	21.5	0.97	14.202±0.304	136830±2926	121286±2594
PR109	35°37′	94°11.6′	4967	21.5	0.97	13.605±0.227	130900±2180	116505±1940
PR110	35°36′	94°9.8′	4880	20.65	0.97	22.609±0.390	231714±3992	204451±3522
PR111	35°36′	94°9.8′	4887	20.72	0.97	18.564±0.314	187763±3172	168033±2838
PR112	35°36′	94°9.8′	4882	20.67	0.97	21.405±0.354	218514±3617	193131±3197
PR113	35°36′	94°9.8′	4884	20.69	0.97	21.657±0.364	221009±3718	195115±3282
PR114	35°43′	94°15.4′	4466	17.03	0.97	9.655±0.162	116926±1962	105322±1767
PR115	35°43′	94°15.4′	4460	16.98	0.97	7.404±0.266	89358±3205	81978±2941
PR116	35°43′	94°15.5′	4476	17.11	0.97	7.722±0.188	92538±2251	84900±2066
PR117	35°43′	94°15.4′	4457	16.95	0.97	5.609±0.192	67449±2305	62077±2121
PR125	35°37′	94°11.8′	5018	22.01	0.97	7.727±0.098	71636±904	65694±829
PR126	35°37′	94°11.8′	5018	22.01	0.97	6.942±0.097	64253V901	59159±829
PR127	35°37′	94°11.8′	5015	21.98	0.97	11.739±0.209	109943±1962	99701±1779
PR128	35°37′	94°11.8′	5013	21.96	0.97	9.202±0.203	85789±1891	78587±1732
PR131	36°18′	94°47.6′	2849	7.17	0.97	1.511±0.060	42739±1684	39272±1547
PR132	36°18′	94°47.6′	2849	7.17	0.97	1.120±0.034	31587±967	30135±922

[a]Corrected for paleomagnetic variaions using data from Ohno and Hamano (1992), McEllhinny and Senanayake (1982) and the SINT-800 record (Guyodo and Valet, 1999).

these high-energy mountainous environments is probably in the order of a few hundred to several thousand years (cf. Puktonen and Swanson, 2003; Barnard et al., 2004a, b).

The SEDs for boulders on landforms on the southern side of the Burhan Budai Shan range from >232 to 11 ka, with a large number being well older than 100 ka. This

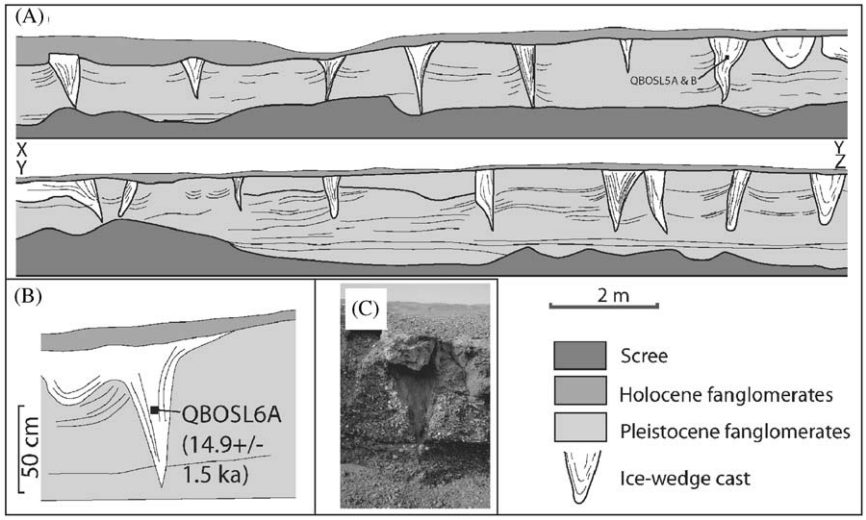

Fig. 11. Ice-wedge casts showing the OSL dating that has been undertaken at Lenghu (38 °51.229′N/093 °25.077′E 2782 m asl).

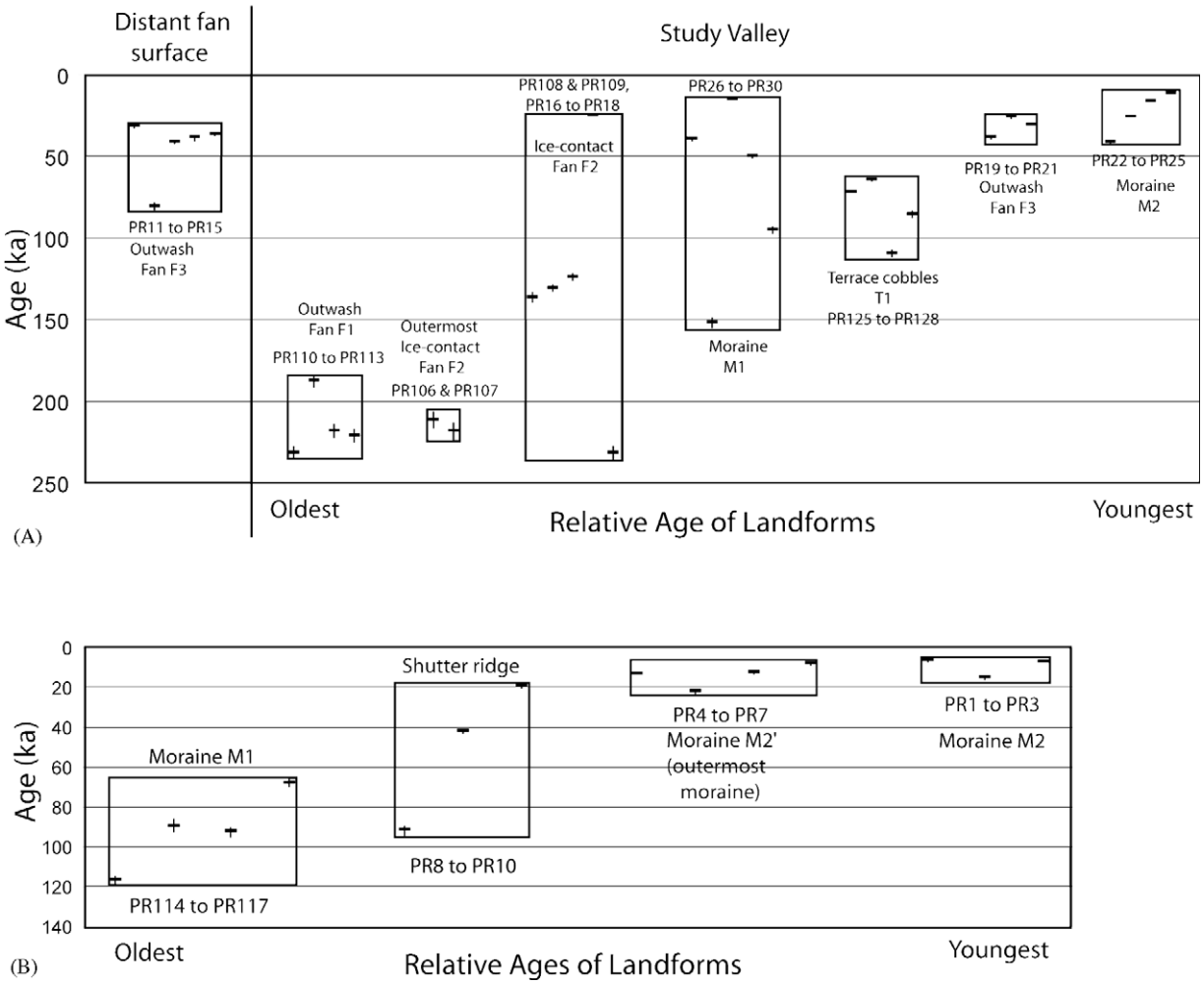

Fig. 12. Be-10 terrestrial cosmogenic radionuclide surface exposure dates plotted by relative age of the landforms for (A) the landforms south of Burhan Budai Shan and (B) the landforms south of Burhan Budai Shan.

suggests that many of the landforms that we have dated formed during or before the penultimate glacial cycle. Landforms of such antiquity are prone to erosion and it is rare for boulders on their surfaces to remain stable through the whole history of the landform. This results in a large scatter of SEDs on individual landforms, and the older

ages in each data set are probably more indicative of the true age of the landform.

Such scatter of ages is evident for outwash fan F1 whose boulders have SEDs which range from 232 to 188 ka. However, with the exception of PR111 (188 ka), all the other boulders are >200 ka. Given the likelihood that the boulders on this fan have undergone significant weathering, the fan is likely to be much older than 200 ka.

Ice-contact fan F2 provides another example of the large scatter of SEDs, which range from 124 to 232 ka. With the exception of PR17 (~25 ka), however, all the boulders on the F2 ice-contact fan surfaces are much older than 100 ka. This suggests that they formed during the penultimate glacial cycle. The moraine that is associated with these fans has SEDs with an exceptionally large range (15–152 ka). Given the effect of weathering and toppling of boulders on a moraine crest, together with possible exhumation as the moraine degrades with time, the older ages in the data set suggest that it likely formed during the penultimate glacial cycle, coincident with the F2 ages that suggest formation during the penultimate glacial cycle.

The scatter of SEDs on outwash fan F3 dates in the distal area is large (32–81 ka), but much less for the study valley (26–39 ka). The old age of PR12 suggests that it is likely that this boulder fell from a stratigraphically higher and older location. If PR12 (~81 ka) is excluded from the data set, the SEDs cluster between 26 and 39 ka suggesting that these outwash fans formed during MIS-3.

Terrace T1 has SEDs that range from 64 to 110 ka, which suggest that it formed during the early part of the last glacial cycle. However, morphostratigraphically it is younger than F3, which suggests that either the cobbles on T1 had significant inherited Be-10 from prior exposure or that the boulders on F3 ages are too young, a consequence of weathering or exhumation.

M2 has SEDs that range from 41 to 11 ka. Although we cannot equivocally assign an age to this moraine, it is possible that this moraine formed during MIS-3, and it is associated with the F3 outwash fan.

On northern side of Burhan Budai Shan, the oldest moraine (M1) has SEDs that range from 117 to 67 ka, while the younger moraines have SEDs that range from 22 to 6 ka. Boulders on the shutter ridge have ages that range from 92 to 19 ka. The large spread of dates might be the consequence of burial by aeolian silts and recent exhumation. The M1 moraines may represent an advance during the early part of the last glacial cycle or even during the penultimate glacial cycle. These moraines are probably equivalent to an early stage of Lui et al.'s (2006) Yuzhufeng Glaciation, but the dates are clearly older than the ESR and TL dates that they present. The M2 moraines are likely to represent an advance during the Last Glacial Maximum (LGM) or Lateglacial. However, they may even represent a Holocene glacial advance, with the older dates representing derived boulders. These moraines are probably equivalent to a late stage of Lui et al.'s (2006) Yuzhufeng Glaciation. The Holocene ages on the alluvial fans dated by Van der Woerd et al. (2002) suggest that there were significant climatic and hydrological cycles throughout the Holocene, and many of the alluvial fans/terraces might have a paraglacial origin. The ages on the shutter ridge support the view that there was no extensive trunk valley glaciation during the last glacial cycle. If there had been such a glaciation, it would be difficult to explain the old SEDs. The moraines near the present glacial have not been dated and their freshness suggests that they formed during the Late Holocene.

The alluvial fans along Burhan Budai-Golmud drainage that were dated using SED and OSL techniques have ages that range from 43 to 8 ka. The most distal alluvial fan surface that was dated (Section Z, Fig. 7) has SEDs that range between 43 and 33 ka (PR131 and 132) while Section Y that is correlated to this surface, ~50 km south, has a SED of ~32 ka (PR103; Fig. 7). This latter date is supported by an OSL date of 28.3 ± 2.8 ka on sediments within the alluvial fan. Another contemporaneous alluvial fan surface, ~30 km to the south (Site A, Fig. 7) has boulders on it that date from 25 to 10 ka (PR100–102). The large range of ages for boulders on this surface might be attributed to exhumation and or burial at this site. The correlated alluvial fan surface (Section X, Fig. 7) has an OSL date on fanglomerates of 26.3 ± 2.4 ka. The fanglomerates at this site are capped with swamping/lacustrine silts and have an OSL age of 8.8 ± 0.8 ka. These are in turn overlain by loess. The thickest loess section that was examined in the field had a basal OSL date of 8.6 ± 0.7 ka. These data suggest that the main alluvial fans which form the major component of the valley fills along the Burhan Budai-Golmud drainage were forming and infilling the valley during MIS-3 and that they became abandoned/incised prior MIS-2. Later sedimentation as shallow pond and loess probably occurred during and since the early Holocene.

The OSL date of 14.9 ± 1.5 ka on the aeolian sediments within the ice wedge cast at Lenghu suggests significant climatic amelioration during the Lateglacial, with the degradation of basin permafrost conditions within the Qaidam Basin.

5. Discussion

The pattern of landscape development across the Burhan Budai Shan is asymmetric, the northern slopes and associated valleys to the north, draining into the Qaidam Basin, are clearly more geomorphically dynamic than those to the south that stretch into the main plateau regions of Tibet, where alluvial fans dating to more than 200 ka are preserved. This likely explains why the moraine record on the southern side of the Burhan Budai Shan is more complete than on the northern more active side of the range.

The preliminary analysis of landforms and dating shows a complex and long history of landscape evolution in the Burhan Budai Shan. We have been able to date

depositional landforms back to >200 ka. The geomorphic complexity of this region produces scattered SEDs on individual landforms, making it difficult to assign particular climatostragraphic times to a given formation. Our study illustrates the need for numerous dates and multiple dating techniques to define the ages of landforms and sediments in this environment. The record of paleoenvironmental change and landscape evolution is highly compressed because of continued erosion and resedimentation of landforms and sediments. The large spread of SEDs on individual landform surfaces testifies to this view. The view that the paleoenvironmental record is highly compressed is supported by the scarcity of multiple moraine successions on either side of the Burham Budai Shan. For example, only three sets of moraines are recognized on either side of the mountain range. On the southern side of the Burham Budai Shan, we suggest these date to the penultimate glacial cycle, MIS-3, and an undated moraine which may be LGM, Lateglacial or Holocene. Similarly the moraines on the northern side of the Burham Budai Shan date to penultimate/early last glacial cycle, the LGM/Lateglacial and Holocene. In spite of this lack of precision, our dating of moraines shows that during at least the last two glacial cycles, glaciers only extended a few kilometers into the forelands of the Burham Budai Shan. This observation adds further credence to the view that an extensive ice sheet did not cover the Tibetan Plateau during the Late Quaternary (Derbyshire, 1987; Zheng, 1989; Pu 1991; Hövermann et al., 1993a, b; Rutter, 1995; Lehmkuhl, 1995, 1998; Lehmkuhl et al., 1998; Zheng and Rutter 1998; Zhou and Li, 1998; Schäfer et al., 2002; Owen et al., 2003c). It is likely that older moraines are buried beneath the alluvial fans and/or were resedimented to form part of the thick valley fill that exists along the valleys into the Qaidam Basin. Wu et al. (2001) presents data on buried tills near the Kunlun Pass where the Lhasa-Golmud highway crosses the Burham Budai Shan.

Our dating of the alluvial fans within the Kunlun and extending into the Qaidam Basin shows several distinct phases of sedimentation. The oldest alluvial fan surfaces are preserved on the southern side of the Kunlun and date back >200 ka. A younger set dates to the penultimate glacial cycle and is clearly related to a glacial event because it preserves an ice contact slope along its northern edge which is traceable to moraine M1. A third set of alluvial fans on the southern side of the Burham Budai Shan have SEDs which suggest it formed during MIS-3. The extensive alluvial fans that form the main valley fills along the Burham Budai Shan have similar ages and appear to have become cannibalized during the latter part of MIS-3. The lack of multiple successions of moraines and the substantial thickness of valley fills in the region suggests that many of the moraines have been eroded and resedimented during MIS-3 and/or during earlier times. The lacustrine record from the Qaidam and adjacent lakes, such as Qinghai Lake, show that lake levels were much higher during MIS-3 as a consequence of higher precipitation (Lister et al., 1991; Shi et al., 2001). Glacier reconstructions from adjacent glaciated regions of Tibet suggest that glaciers also grew during this time (Owen et al., 2003a, b, c, 2005). Towards the end of MIS-3, however, the region became more arid and lake levels dropped. It is likely, that falling lake levels lowered the erosional base level, which led to fan incision.

The ice wedge casts at Lenghu provide evidence of permafrost conditions and mean annual air temperatures below −6 °C in the basin prior to ~15 ka. With climatic amelioration, the ground warmed and aeolian sediment was deposited within the casts as the ice wedges melted. Since then, incision and aeolian deposition have dominated the environment. This sequence and timing of events is remarkably similar to that found by Owen et al. (1998) in the Gobi Desert of Mongolia and by Porter et al. (2001) along the southern shores of Qinghai Lake. The substantial caps of loess that are present along the Golmud-Xidatan drainage are further for a period of climatic amelioration during the Holocene. The basal dates in the section that we examined suggest that the Holocene loess deposition started at 8 ka. Despite finding one of the thickest deposits of loess, we may have been unlucky and did not find the oldest loess deposit in region.

6. Conclusions

Our field mapping, geomorphic and sedimentological analysis, and dating define at least three glacial advances in the Burham Budai Shan of the Kunlun Mountains. On the northern side of the Burham Budai Shan, these advances date to penultimate/early last glacial cycle, the LGM/Lateglacial and Holocene, while on the south side of the range, these dates to the penultimate glacial cycle, MIS-3, and possibly the LGM, Lateglacial or Holocene.

Several distinct phases of alluvial fan sedimentation are defined and include alluvial fans on the southern side of the Kunlun that date to >200 ka, a younger set of ice-contact fan that date to the penultimate glacial, and a third set of fans which formed during MIS-3. Extensive incised alluvial fans that form the main valley fills along Xidatan-Golmud drainage, have depositional and surface exposure ages that date to ~30 ka. This suggests that there was a period of alluvial fan aggradation and valley filling that was persistent prior to ~30 ka. The desiccation of the large lakes in the Qaidam Basin post ~30 ka likely led to base level lowering and active incision of streams into the valley fills. The continued Lateglacial and Holocene desiccation probably led to further degradation of the valley fills. Aeolian sediments that comprise ice wedge casts in the Qaidam Basin have OSL dates of ~15 ka indicating significant climatic amelioration. Holocene loess caps most landforms north of the Burhan Budai and the thickest deposit we found has a basal OSL date of ~8 ka suggesting increasing aridity in the region since the early Holocene.

Our study provides a framework to define the timing of formation of Late Quaternary landforms along the

southern and northwestern margins of the Qaidam Basin, and in the Burhan Budai Shan of the Kunlun Mountains, and strongly suggests links between climatic amelioration, deglaciation, lake desiccation and alluvial fan evolution. From these observations, we believe that the major landscape changes that occur within high glaciated mountains and their adjacent hyper-arid intermontane basins, such as the Kunlun Mountains and Qaidam Basin, occur rapidly over millennial timescales during periods of climatic instability. However, the region is tectonically active and we can rule out the possible tectonic influences on sedimentation and landscape evolution during the Late Quaternary. We highlight that this region provides an ideal natural laboratory to examine the interaction between tectonics and climate within a continent–continent collision zone and to quantify rates of landscape evolution as controlled by climate and the associated glacial and hydrological changes in hyper-arid and adjacent high-altitude environments. Our study, particularly the numerical dating, is a first step in helping to quantify the rates of change in this environment.

Acknowledgments

This work was performed under the auspices of the US Department of Energy by the University of California, Lawrence Livermore National Laboratory under DOE contract W-7405-ENG-48) and as part of an IGPP/LLNL research grant. We also thank Yingkui Li and Marc Caffee for their constructive reviews of this paper.

References

Adamiec, G., Aitken, M., 1998. Dose-rate conversion factors: update. Ancient TL 16, 37–50.

Aitken, M.J., 1998. An introduction to optical dating. Oxford University Press, Oxford.

Barnard, P.L., Owen, L.A., Finkel, R.C., 2004a. Style and timing of glacial and paraglacial sedimentation in a monsoonal influenced high Himalayan environment, the upper Bhagirathi Valley, Garhwal Himalaya. Sedimentary Geology 165, 199–221.

Barnard, P.L., Owen, L.A., Sharma, M.C., Finkel, R.C., 2004b. Late Quaternary (Holocene) landscape evolution of a monsoon-influenced high Himalayan valley, Gori Ganga, Nanda Devi, NE Garhwal. Geomorphology 61, 91–110.

Benn, D.I., Owen, L.A., 2002. Himalayan glacial sedimentary environments: a framework for reconstructing and dating former glacial extents in high mountain regions. Quaternary International 97–98, 3–26.

Bortolot, V.J., 1997. Improved OSL excitation with fiber optics and focused lamps. Radiation Measurements 27, 101–106.

Brantingham, P.J., Olsen, J.W., Schaller, G.B., 2001. Lithic assemblages from the Chang Tang region, Northern Tibet. Antiquity 75, 319–327.

Brantingham, P.J., Ma, H., Olsen, J.W., Guo, X., Madsen, D.B., Rhodes, D.E., 2003. Speculation on the timing and nature of Late Pleistocene hunter-gatherer colonization of the Tibetan Plateau. Chinese Science Bulletin 48, 1510–1516.

Chen, K., Bowler, J.M., 1986. Late Pleistocene evolution of salt lakes in the Qaidam Basin, Qinghai Province, China. Palaeogeography, Palaeoclimatology, Palaeoecology 54, 87–104.

Derbyshire, E., 1987. A history of the glacial stratigraphy in China. Quaternary Science Reviews 6, 301–314.

Derbyshire, E., Owen, L.A., 1990. Quaternary alluvial fans in the Karakoram Mountains. In: Rachocki, A.H., Church, M. (Eds.), Alluvial Fans: A Field Approach. Wiley, New york, pp. 27–53.

Farber, D.L., Hancock, G.S., Finkel, R.C., Rodbell, D., 2005. The age and extent of tropical glaciation in the Cordillera Blanca, Peru. Journal of Quaternary Science 20, 759–776.

Finkel, R.C., Owen, L.A., Barnard, P.L., Caffee, M.W., 2003. Beryllium-10 dating of Mount Everest moraines indicates a strong monsoonal influence and glacial synchroneity throughout the Himalaya. Geology 31, 561–564.

Hövermann, J., Lehmkuhl, F., Pörtge, K.-H., 1993a. Pleistocene glaciations in Eastern and Central Tibet- Preliminary results of the Chinese–German joint expeditions. Zeitschrift für Geomorphologie 92, 85–96.

Hövermann, J., Lehmkuhl, F., Süssenberger, H., 1993b. Neue Befunde zur Paläoklimatologie Nordafrikas und Zentralasiens. Abhandlungen der Braunschweigischen Wissenschaftlichen Gesellschaft 43, 127–150.

Kohl, C.P., Nishiizumi, K., 1992. Chemical isolation of quartz for measurement of in-situ-produced cosmogenic nuclides. Geochimica et Cosmochimica Acta 56, 3583–3587.

Lal, D., 1991. Cosmic ray labeling of erosion surfaces: in situ nuclide production rates and erosion models. Earth and Planetary Science Letters 104, 429–439.

Lal, D., Peters, B., 1967. Cosmic ray produced radioactivity on the Earth. In: Flugge, S. (Ed.), Handbuch der Physik, vol. 4612, pp. 551–612.

Lehmkuhl, F., 1995. Geomorphologische Untersuchungen zum Klima des Holozäns und Jungpleistozäns Osttibets. Göttinger Geographische Abhandlungen 102, 1–184.

Lehmkuhl, F., 1998. Extent and spatial distribution of Pleistocene glaciations in Eastern Tibet. Quaternary International 45/46, 123–134.

Lehmkuhl, F., Owen, L.A., Derbyshire, E., 1998. Late Quaternary glacial history of Northeastern Tibet. In: Owen, L.A. (Ed.), Mountain Glaciations Quaternary Proceedings, 6, pp. 121–142.

Lister, G.S., Kelts, K., Chen, K.Z., Jun-Qing, Y., Niessen, F., 1991. Lake Qinghai, China: closed-basin lake levels and the oxygen isotope record for ostracoda since the latest Pleistocene. Palaeogeography, Palaeoclimatology, Palaeoecology 84, 141–162.

Lui, G., Zhang, X., Cui, Z., Wu, Y. Fu, H., Wei, X., 2006. A review of glacial sequences of the Kunlun Pass, northern Tibetan Plateau. Quaternary International, this volume.

Masarik, J., Wieler, R., 2003. Production rates of cosmogenic nuclides in boulders. Earth and Planetary Science Letters 216, 201–208.

Mejdahl, V., 1979. Thermoluminescence dating: beta attenuation in quartz grains. Archaeometry 21, 61–73.

Murray, A.S., Wintle, A.G., 2000. Luminescence dating of quartz using an improved single-aliquot regenerative-dose protocol. Radiation Measurements 32, 57–73.

Nishiizumi, K., Finkel, R.C., Klein, J., Kohl, C.P., 1996. Cosmogenic production of 7Be and 10Be in water targets. Journal of Geophysical Research 101, 22,225–22,232.

Owen, L.A., Richards, B., Rhodes, E.J., Cunningham, W.D., Windley, B.F., Badamgarav, J., Dorjnamjaa, D., 1998. Relic permafrost structures in the Gobi of Mongolia: age and significance. Journal of Quaternary Science 13, 539–548.

Owen, L.A., Gualtieri, L., Finkel, R.C., Caffee, M.W., Benn, D.I., Sharma, M.C., 2001. Cosmogenic radionuclide dating of glacial landforms in the Lahul Himalaya, Northern India: defining the timing of Late Quaternary glaciation. Journal of Quaternary Science 16, 555–563.

Owen, L.A., Finkel, R.C., Caffee, M.W., Gualtieri, L., 2002a. Timing of multiple glaciations during the Late Quaternary in the Hunza Valley, Karakoram Mountains, Northern Pakistan: defined by cosmogenic radionuclide dating of moraines. Geological Society of America Bulletin 114, 593–604.

Owen, L.A., Finkel, R.C., Caffee, M.W., 2002b. A note on the extent of glaciation in the Himalaya during the global Last Glacial Maximum. Quaternary Science Reviews 21, 147–157.

Owen, L.A., Kamp, U., Spencer, J.Q., Haserodt, K., 2002c. Timing and style of Late Quaternary glaciation in the eastern Hindu Kush, Chitral, northern Pakistan: a review and revision of the glacial chronology based on new optically stimulated luminescence dating. Quaternary International 97–98, 41–56.

Owen, L.A., Spencer, J.Q., Ma, H., Barnard, P.L., Derbyshire, E., Finkel, R.C., Caffee, M.W., Zeng Yong, N., 2003a. Timing of Late Quaternary glaciation along the southwestern slopes of the Qilian Shan. Boreas 32, 281–291.

Owen, L.A., Ma, H., Derbyshire, E., Spencer, J.Q., Barnard, P.L., Zeng, Y.N., Finkel, R.C., Caffee, M.W., 2003b. The timing and style of Late Quaternary glaciation in the La Ji Mountains, NE Tibet: evidence for restricted glaciation during the latter part of the Last Glacial. Zeitschrift für Geomorphologie 130, 263–276.

Owen, L.A., Finkel, R.C., Ma, H., Spencer, J.Q., Derbyshire, E., Barnard, P.L., Caffee, M.W., 2003c. Timing and style of Late Quaternary glaciations in NE Tibet. Geological Society of America Bulletin 15, 1356–1364.

Owen, L.A., Finkel, R.C., Barnard, L.P., Ma, H., Ashai, K., Caffee, M.W., Derbyshire, E., 2005. Climatic and topographic controls on the style and timing of Late Quaternary glaciation throughout Tibet and the Himalaya. Quaternary Science Reviews 24, 1391–1411.

Pigati, J.S., Lifton, N.A., 2004. Geomagnetic effects on time-integrated cosmogenic nuclide production with emphasis on in situ C-14 and Be-10. Earth and Planetary Science Letters 226, 193–205.

Porter, S.C., Singhvi, A., An, Z., Lai, Z., 2001. Luminescence age and paleoenvironmental implications of a Late Pleistocene ground wedge on the northeastern Tibetan Plateau. Permafrost and Periglacial Processes 12, 203–210.

Prescott, J.R., Hutton, J.T., 1994. Cosmic ray contributions to dose rates for luminescence and ESR dating: Large depths and long-term time variations. Radiation Measurements 23, 497–500.

Prescott, J.R., Stephans, L.G., 1982. Contribution of cosmic radiation to environmental dose. PACT 6, 17–25.

Pu, Q., 1991. Quaternary glaciers in China. In: Zhang, Z., Shao, S., Tong, G., Cao, J. (Eds.), The Quaternary of China. China Ocean Press, Beijing, pp. 240–273.

Putkonen, J., Swanson, T., 2003. Accuracy of cosmogenic ages for moraines. Quaternary Research 59, 255–261.

Richards, B.W.M., Benn, D.I., Owen, L.A., Rhodes, E.J., Spencer, J.Q., 2000a. Timing of Late Quaternary glaciations south of Mount Everest in the Khumbu Himal, Nepal. Geological Society of American Bulletin 112, 1621–1632.

Richards, B.W., Owen, L.A., Rhodes, E.J., 2000b. Timing of Late Quaternary glaciations in the Himalayas of northern Pakistan. Journal of Quaternary Science 15, 283–297.

Rutter, N.W., 1995. Problematic ice sheets. Quaternary International 28, 19–37.

Schäfer, J.M., Tschudi, S., Zhizhong, Z., Xihao, W., Ivy-Ochs, S., Wieler, R., Baur, H., Kubik, P.W., Schluchter, C., 2002. The limited influence of glaciations in Tibet on global climate over the past 170000 yr. Earth and Planetary Science Letters Earth and Planetary Science Letters 194, 287–297.

Shi, Y., Yu, G., Liu, X., Li, B., Yao, T., 2001. Reconstruction of the 30–40 ka BP enhanced Indian monsoon climate based on geologic records from the Tibetan Plateau. Palaeogeography, Palaeoclimatology, Palaeoecology 169, 69–83.

Stone, J.O., 2000. Air pressure and cosmogenic isotope production. Journal of Geophysical Research 105, 23,753–23,759.

Van der Woerd, Tapponnier, P., Ryerson, F.J., Meriaux, A.-S., Meyer, B., Gaudemer, Y., Finkel, R.C., Caffee, M.W., Zhao, G., Xu, Z., 2002. Uniform postglacial slip-rate along the central 600 km of the Kunlun Fault (Tibet), from ^{26}Al, ^{10}Be, and ^{14}C dating of riser offsets, and climatic origin of the regional morphology. Geophysical Journal International 148 356–388.

Wang, J., Derbyshire, E., Shaw, J., 1986. Preliminary magnetostratigraphy of Dabusan Lake, Qaidam Basin, central Asia. Physics of the Earth and Planetary Interiors 44, 41–46.

Wu, Y., Cui, Z., Liu, G., Ge, D., Yin, J., Xu, Q., Pang, Q., 2001. Quaternary geomorphological evolution of the Kunlun Pass area and uplift of the Qinghai-Xizang (Tibet) Plateau. Geomorphology 36, 203–216.

Zheng, B., 1989. Controversy regarding the existence of a large ice sheet on the Qinghai-Xizang (Tibetan) Plateau during the Quaternary Period. Quaternary Research 32, 121–123.

Zheng, B., Rutter, N., 1998. On the problem of Quaternary glaciations, and the extent and patterns of Pleistocene ice cover in the Qinghai-Xizang (Tibet) plateau. Quaternary International 45/46, 109–122.

Zhou, S., Li, J., 1998. The sequence of Quaternary glaciation in the Bayan Har Mountains. Quaternary International 45/46, 135–142.

Zimmerman, D.W., 1971. Thermoluminescent dating using fine grains from pottery. Archaeometry 13, 29–52.